Three-Dimensional Evolution of Large-Amplitude Internal Waves in the Strait of Gibraltar

VASILIY VLASENKO

SEOES, University of Plymouth, Plymouth, United Kingdom

JOSE C. SANCHEZ GARRIDO

Grupo de Oceanografia Fisica, University of Malaga, Malaga, and Grupo de Puertos y Costas, University of Granada, Granada, Spain

NATALIYA STASHCHUK

SEOES, University of Plymouth, Plymouth, United Kingdom

JESUS GARCIA LAFUENTE

Grupo de Oceanografia Fisica, University of Malaga, Malaga, Spain

MIGUEL LOSADA

Grupo de Puertos y Costas, University of Granada, Granada, Spain

(Manuscript received 26 February 2008, in final form 17 March 2009)

ABSTRACT

The modeling of large-amplitude internal waves (LAIWs) propagating in the Strait of Gibraltar is carried out using a fully nonlinear nonhydrostatic numerical model. The focus of the modeling efforts was on three-dimensional peculiarities of LAIW evolution, namely, cross-strait variability, interaction with lateral boundaries (including wave breaking and water mixing), radiation of secondary waves from orographic features, and interaction of secondary scattered internal waves.

The along-channel propagation of packets of LAIWs reveals remarkable three-dimensional behavior. Due to the Coriolis force and multiple reflections from the lateral boundaries, the largest leading LAIW loses its energy much faster than that in the packet tail, which captures the scattered energy from the leading wave as it propagates and grows in amplitude. As a result of the energy transfer, the initially rank-ordered wave packet loses its regular structure to evolve into a non-rank-ordered wave train. In situ data collected in the eastern part of the Strait of Gibraltar confirm the idea that the non-rank-ordered structure is a common feature of internal wave packets emerging from the strait into the Alboran Sea.

1. Introduction

Large-amplitude internal waves (LAIWs) are one of the most striking phenomena observed in the Strait of Gibraltar. These waves appear as packets propagating along the strait to evolve into groups of well-separated solitary waves entering the Alboran Sea. The mechanism of their generation has been described in many papers (e.g., Armi and Farmer 1988; Brandt et al. 1996; Izquierdo et al. 2001; Bruno et al. 2002; Vazquez et al. 2005). According to these investigations, LAIWs observed in the strait are the result of the nonlinear evolution of a baroclinic bore generated by a barotropic tidal flow over Camarinal Sill (CS); see Fig. 1. The waves have several hundred meters of wavelength and vertical displacements of 100 m or more (Wesson and Gregg 1988). Nonlinear wave theory suggests that a propagating baroclinic bore normally disintegrates into a packet of well-rank-ordered solitary internal waves (Whitham

Corresponding author address: Vasiliy Vlasenko, School of Earth, Ocean and Environmental Sciences, University of Plymouth, Drake Circus, Plymouth PL8 4AA, United Kingdom.
E-mail: vvlasenko@plymouth.ac.uk

DOI: 10.1175/2009JPO4007.1

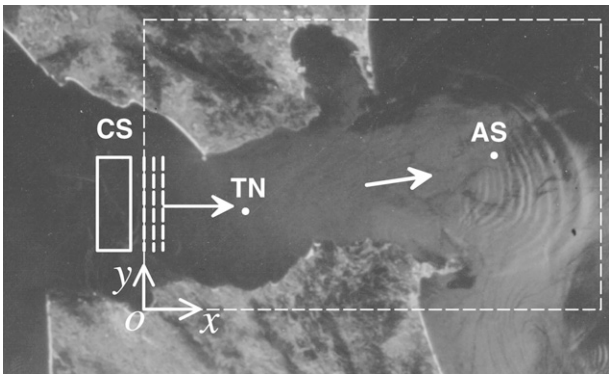

FIG. 1. Sea surface manifestation of a wave packet of LAIWs propagating from the strait toward the Alboran Sea [courtesy of the European Space Agency (ESA)]: CS is Camarinal Sill; TN and AS denote the locations of the moorings deployed at Tarifa Narrow and in the Alboran Sea.

(1974); Apel (2003)). However, not all observational data support this theoretical result. In many cases measurements reveal an irregular rather than a well-ordered structure of packets. In particular, this statement concerns the data collected in the Strait of Gibraltar at positions TN and AS (see Fig. 1).

Figure 2a shows a 5-day temperature series at AS. Packets of LAIWs are clearly identified by the fast temperature oscillations recorded every tidal period [a detailed analysis of these data is presented in Sanchez Garrido et al. (2008)]. Figures 2b–d show that the expected rank-ordered structure is not a necessary attribute of the wave packets observed in the strait. Statistical analysis of all recorded wave trains (46 well-defined packets) reveals that only 46.5% of them can be identified as well-rank-ordered wave trains like that presented in Fig. 2b. The rest, that is, 53.5% of the packets, were either partly rank ordered (23.3%, as presented in Fig. 2c) or irregular rather than organized (30.2%, as in Fig. 2d). A similar conclusion was formulated earlier by La Violette et al. (1986). This empirical fact of a clear tendency to disorder in wave packets was a starting point of the present study.

There are several possible reasons for the discrepancy between theoretical predictions and real observations. One of these is the wave refraction over the complex bottom topography, which in some cases can be studied using linear geometrical optics. More sophisticated methods are required for the investigation of the refraction of strongly nonlinear internal waves when wave breaking, water mixing, generation of higher baroclinic modes, nonlinear wave dispersion, wave–wave interaction, and some other nonlinear effects can develop. Among them, we could mention the use of the higher-order weakly nonlinear equations like the extended Korteweg–de Vries (KdV) equation (Grimshaw et al.

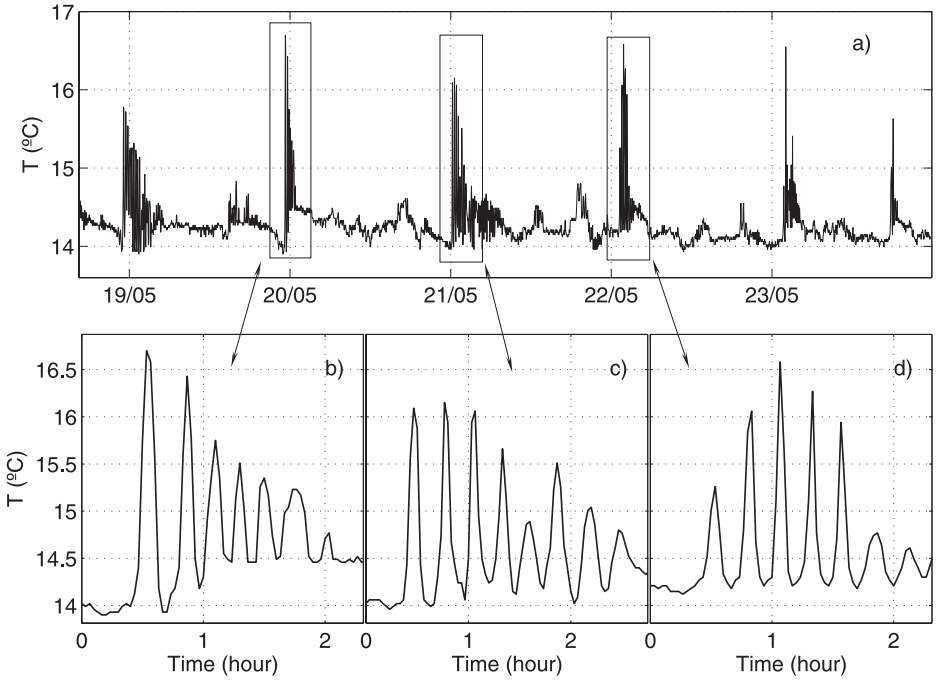

FIG. 2. (a) A fragment of the temperature time series recorded at the AS mooring 85-m depth (see Fig. 1). Zoom-ins: Details of three particular fragments representing (b) well-organized, (c) partly rank-ordered, and (d) non-rank-ordered packets of LAIWs.

2002, 2004), the rotation-modified Kadomtsev–Petviashvili equation (Grimshaw and Melville 1989; Grimshaw and Tang 1990; Grimshaw et al. 1998), or even fully nonlinear three-dimensional (3D) nonhydrostatic numerical models (Vlasenko and Stashchuk 2007).

We hypothesize here that the irregular structure of the wave packets observed in the Strait of Gibraltar is the manifestation of a sophisticated 3D mechanism of interaction of LAIWs with the lateral boundaries of the rotating strait where wave refraction and reflection, extensive wave breaking, and water mixing take place. Being repeated many times in every wave packet, these processes produce a complex spatial structure in which wave energy is transferred from wave to wave or converted into turbulence. The goal of this paper is to study the 3D evolution of LAIWs in the strait and to describe the pathway of the energy in order to explain the irregular structure of the observed wave packets. The paper is organized as follows: the model and its initialization are described in section 2, section 3 presents the basic set of numerical experiments, and a discussion, comparison with observational data, and the conclusions are included in section 4. In appendix A, we summarize the procedure of energy calculation, while in appendix B we discuss the influence of the mean flow.

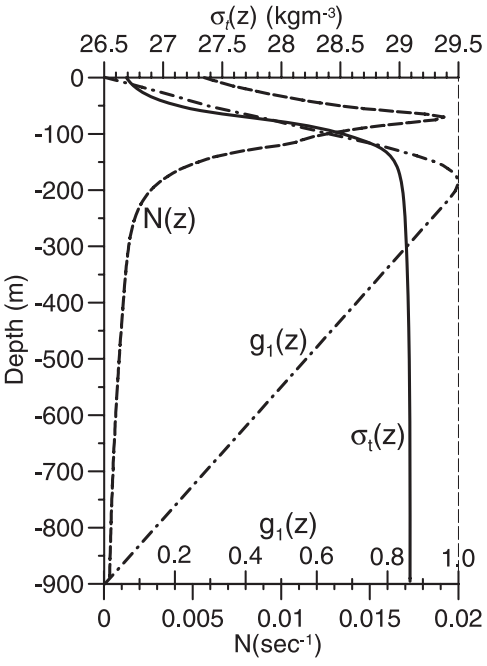

FIG. 3. Typical density (solid line), buoyancy frequency (dashed line), and vertical wave displacement (dashed-point line) profiles at mooring TN.

2. Model description and initialization

The model domain presented by the dashed rectangle in Fig. 1 includes a 61 km × 42 km sector of irregular bottom topography and shoreline. Consider the Cartesian system of coordinates, xyz, with $0xy$ within the undisturbed free surface and the $0z$ axis directed vertically upward, while the $0x$ axis is eastward and the $0y$ axis northward. It is assumed that LAIWs observed in the strait are the result of disintegration of a baroclinic bore generated by the barotropic tide interacting with Camarinal Sill (solid rectangle in Fig. 1). The baroclinic bore propagates eastward along the strait and disintegrates into a packet of solitary waves, which further enter the Alboran Sea, as presented on the synthetic aperture radar image in Fig. 1. The details of the bore generation and disintegration are not addressed in this paper, which focuses only on the evolutionary stage of the tidally generated LAIWs. The task is split into two subtasks: (i) the first step is the model initialization, that is, the preparation of the initial field of solitary LAIWs, and (ii) the second objective is to study the wave evolution itself when the LAIWs propagate along the strait and interact with the 3D bottom topography and shoreline.

The Massachusetts Institute of Technology general circulation model (MITgcm) was used for both problems. The MITgcm (Marshall et al. 1997) solves the nonhydrostatic, nonlinear equations and has a free-surface formulation, allowing one to trace the position of the solitary waves in (x, y) space. Earth rotation is also taken into account. The model resolution, $\Delta x = 50$ m and $\Delta y = 200$ m, gives more than 40 grid points across the wave. The vertical step, $\Delta z = 7.5$ m in the upper 300-m layer and $\Delta z = 50$ m below it, allows fairly good resolution of the pycnocline. The mean buoyancy frequency profile (Fig. 3) was obtained from the Mediterranean Hydrological Atlas (MEDATLAS) database collected near point TN. According to these historical data, the pycnocline was located at 75-m depth. The bottom topography was extracted from the fine-resolution bottom chart of Sanz et al. (1991) and the shoreline was settled at the 20-m depth contour. No-slip conditions at the bottom and lateral boundaries were used in the model. Assuming strong wave breaking near the lateral boundaries, the Richardson-number-dependent parameterizations (Pacanowski and Philander 1981) of turbulent closure for vertical viscosity ν and diffusivity κ were chosen:

$$\nu = \frac{\nu_0}{(1 + \alpha \mathrm{Ri})^n} + \nu_b, \quad \kappa = \frac{\nu}{(1 + \alpha \mathrm{Ri})} + \kappa_b,$$

where the Richardson number is $\mathrm{Ri} = N^2(z)/(u_z^2 + v_z^2)$; $\nu_b = 10^{-5}$ m^2 s^{-1} and $\kappa_b = 10^{-5}$ m^2 s^{-1} are the background parameters; and $\nu_0 = 1.5 \times 10^{-2}$ m^2 s^{-1}, $\alpha = 5$,

and $n = 1$ are the adjustable parameters. Such a parameterization increases ν and κ in areas where the Richardson number is small. Horizontal diffusivity and viscosity were $10^{-2}\,m^2\,s^{-1}$. As showed by Vlasenko et al. (2005b), with this parameterization the numerical model gives quite robust results even in the case of wave breaking. We set zero value for all wave disturbances at the eastern boundary until the wave reaches it; at this moment the calculations are terminated. At the western boundary the Orlanski-type conditions were used.

An initial plane LAIW of depression (or packet of waves) is set at $t = 0$. According to previous investigations (Vazquez et al. 2005; Sanchez Garrido et al. 2008), the LAIWs generated over Camarinal Sill are trapped there up to 4 h and then they are released and propagate along the channel. They can be identified as solitary waves 4 km to the east of Camarinal Sill. The initial wave or wave packet in the model was taken parallel to the y axis, propagating eastward (see Fig. 1). Such a choice of initial fields is justified by the specific model geometry, which is generally two-dimensional in the area of Camarinal Sill and oriented in the north–south direction so that oscillating east–west barotropic tidal flow produces roughly two-dimensional internal waves propagating eastward, as schematically presented in Fig. 1 by dashed lines.

The procedure for preparation of the initial fields for the incident LAIWs (subtask 1) is described in Vlasenko et al. (2005b). At the first stage, the model is initialized by the first-mode solitary wave of depression obtained from the KdV equation. The KdV solitary waves do not satisfy the fully nonlinear equations if their amplitudes are large. Thus, taking the amplitude of the initial KdV LAIW from the range typically observed in the strait [more than 60 m according to Wesson and Gregg (1988), which is far beyond the applicability of any weakly nonlinear model], we expect a substantial discrepancy using the hydrodynamic equations. Once inserted into the numerical scheme, the strong nonlinear LAIW will evolve, propagating into a basin of constant depth. During this evolution the initial large-amplitude KdV solitary wave is modified, and a new stationary solitary wave is formed at the front of the wave field. The leading wave has the largest amplitude and, as a result, the largest phase speed. This is the reason why this wave detaches from the wave tail and propagates further as an independent internal solitary wave. The model is run until the leading wave separates from the wave tail. The fragment containing the wave is cut from the wave field and used as an initial condition for subtask 2, that is, for the study of its evolution in the strait.

3. Model results

a. One-wave experiments

We start our analysis with the ''one-wave experiment,'' the propagation of one internal solitary wave. This experiment allows one to study the effect of a single wave so that the response in the strait to a wave packet can be treated in terms of a nonlinear superposition of several individual signals. In the first numerical experiment, the amplitude of the incident LAIW was 83 m. The parameter of nonlinearity for this wave, that is, the ratio of the wave amplitude to the depth of the pycnocline, 75 m, is greater than one. The wave evolution is presented in Fig. 4, where the free-surface elevation produced by the internal wave of depression (a few centimeters, in fact) is shown in dark. Note that an internal wave of elevation produces a similar small-scale depression at the free surface (shown in Fig. 4 by light color). Free-surface disturbances are used hereafter as a tracer of spatial structure of the wave fields.

At the initial stage of evolution the incident LAIW retains the characteristics of a plane wave in the domain except for two small regions at the lateral boundaries where the ''edge'' effects of wave–bottom interaction (refraction and breaking) are evident (Fig. 4b). The wave–bottom interaction strengthens over time and, in addition to the refraction and wave breaking, another important process, namely, energy reflection from lateral boundaries, starts to develop in shallow water. As a result of back scattering and dissipation, the propagating LAIW loses energy (the quantitative analysis of wave attenuation is discussed below). This energy leakage, in turn, leads to the formation of secondary internal waves attached to the initial wave (Figs. 4c and 4d). The intensity of wave–topography interaction is stronger to the south, near the African coast, than in the northern part of the strait, near the Spanish coast. The reason is that the Coriolis force transfers energy from the central and northern parts of the wave to the southern boundary of the strait. This behavior has been reported in a number of papers on the structure and evolution of the weakly nonlinear internal solitary waves in idealized channels [see the review by Helfrich and Melville (2006) and references herein]. Figure 4 demonstrates other evidence of this effect but for strongly nonlinear waves, which appear to be more complicated due to the reflection and breaking caused by the irregular bottom topography and coastline. This energy transfer along the wave front does not occur if rotation of the earth is not included in the model (the influence of earth rotation is discussed in the next subsection). At the final stage of evolution the internal waves (both initial and secondary) leave the strait and enter the Alboran Sea (Fig. 4e),

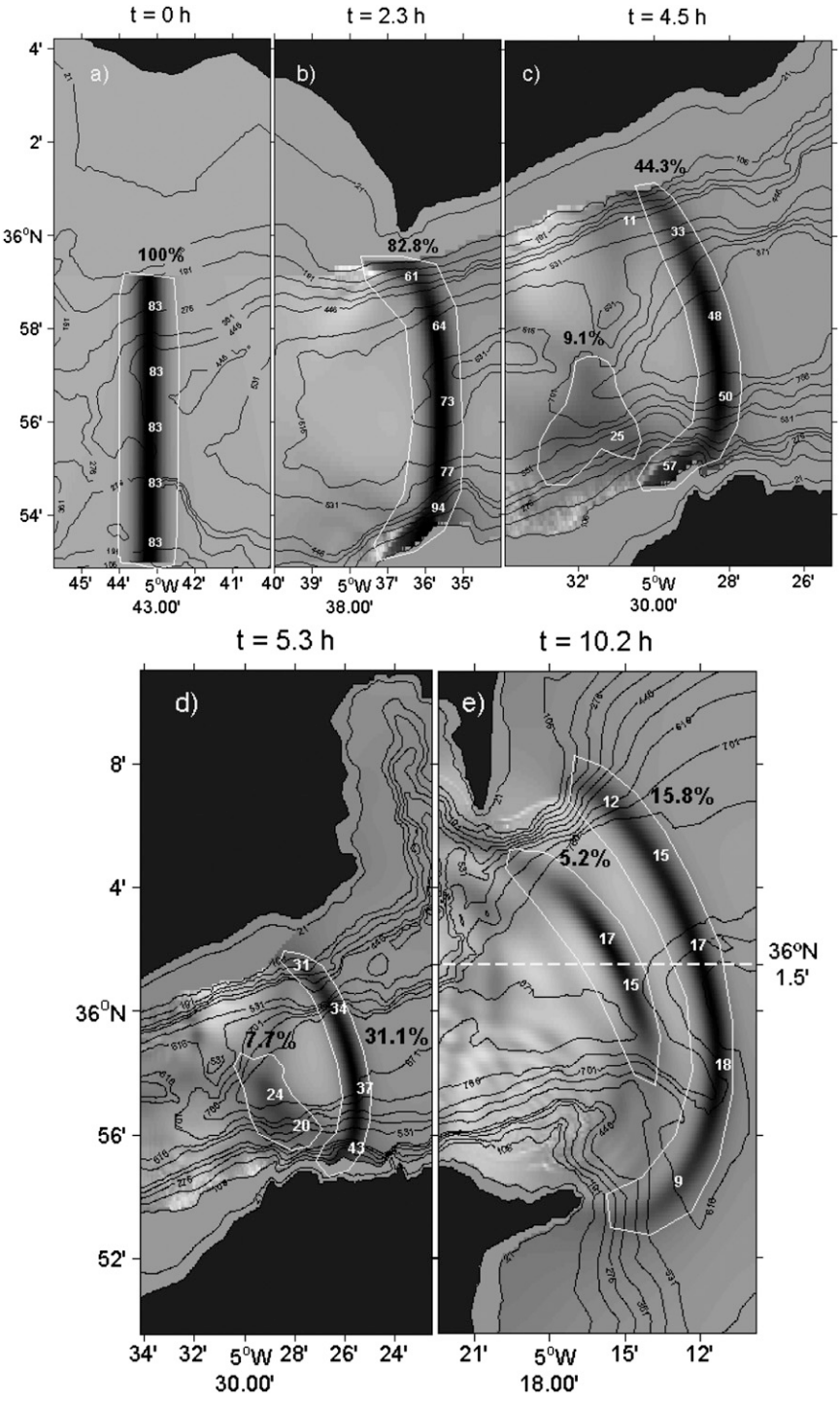

FIG. 4. Sea surface topography produced by the LAIW of depression at different stages of evolution: initial amplitude of the propagating wave is 83 m. Surface elevations and depressions are shown in black and white, respectively; bottom topography is shown by solid lines. The light numbers on the wave fronts represent the wave amplitude (m) at that particular location. The black numbers nearby show the percentage of initial energy inside the area limited by the white contours.

showing spatial structure that recalls the pattern often displayed in satellite images (Fig. 1).

Let us now analyze the spatial structure of scattered internal waves. Figure 4 suggests that these waves are basically formed after the passage of the incident wave through the narrowest part of the strait, that is, the Tarifa Narrows. Eastward of this site the incoming LAIW starts to lose its energy, mostly near the lateral boundaries, due to interaction with the shallow coastal areas. Scrutiny of the 3D wave evolution shows that wave breaking near the strait boundaries is accompanied by wave reflection that, in turn, leads to the formation of secondary scattered waves. The initial stage of this process is shown in Fig. 4c, where the system of two quasi-plane waves reflected from the northern and southern borders of the strait is clearly seen. The superposition of these waves leads to the formation of the ''X type'' spatial structure of the wave fronts, which is typical of the interaction of two obliquely propagating solitary internal waves. Note, however, that this X-type structure is unstable in space and time. After 5.7 h of evolution it has become a fairly stable quasi-plane solitary wave of depression located just behind the leading wave (Fig. 4e). The one-wave experiment initiated by a single incoming LAIW illustrates that the formation of a secondary solitary wave can be explained only in terms of the scattering of the initial wave.

An important characteristic of the wave evolution is its dissipation rate. The white numbers on the wave fronts in Fig. 4 are the local amplitude of internal waves (wave amplitude is assumed to be a vertical excursion of isopycnals at the depth of maximum displacement; see the dotted–dashed line in Fig. 3). Comparison of the wave amplitude at different times indicates the attenuation of the internal wave propagating along the strait: the amplitude in the wave center decreased from 83 (Fig. 4a) to 18 m after 10 hours of evolution (Fig. 4e). The wave damping is more efficient at the wave periphery. For instance, at the end of the simulation the wave amplitude at the southern edge of the wave is less than 10 m. Thus, another conclusion from this experiment is that the wave attenuation depends on the position along the wave front. The wave loses its initial spatial homogeneity and evolves into a wave with higher energy concentration in the central part of the strait.

In terms of energy, the wave attenuation looks even more dramatic (the energy calculation procedure is described in appendix A). Taking the total energy (kinetic and available potential) of the initial LAIW as 100%, we found that after 2.3 h of propagation (Fig. 4b) the LAIW contains only 82.8% of its initial value (the area for energy calculation is shown in Fig. 4b by a white contour). The rest of the energy, that is, 17.2%, is either dissipated due to lateral effects (wave breaking, mixing, viscosity) or transformed into secondary scattered short-scale internal waves located beyond the contour. At the times of the snapshots in Figs. 4c–e, the energy of the leading wave is 44.3%, 31.1%, and 15.8%, respectively, which illustrates a fast dissipation of LAIWs in the strait: the propagating wave could deliver to the Alboran Sea only about 16% of its initial energy.

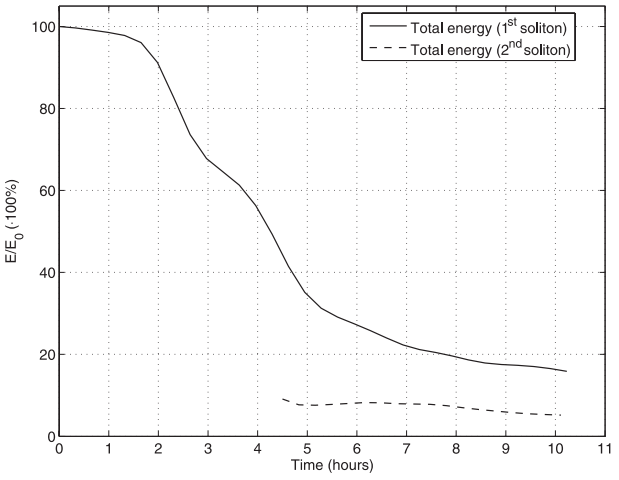

FIG. 5. Time evolution of the total energy of the leading LAIW (solid line) and the generated secondary internal solitary wave (dashed line) normalized by the energy of the initial LAIW. The energy calculation procedure is explained in Fig. 4 and appendix A. The energy of the secondary wave was calculated for $t > 4.5$ h when its shape was clearly identified as a quasi-2D propagating wave.

Figure 5 shows the evolution of the total energy of the leading and the secondary solitary waves. The solid line in Fig. 5 reveals a very fast energy loss by the leading wave during the first 6 hours of evolution. Interestingly, the newly attached secondary wave does not demonstrate similar decay. On the contrary, its energy is basically conserved in the course of the propagation. It looks like the dissipation and reflection from the bottom topography occurring in the leading wave do not apply to the second wave or these processes proceed differently. One possible explanation for its stability could be that the energy dissipated by the second wave is balanced by the gain of energy that has been radiated by the leading LAIW, which brings the energy of both waves to similar values. For instance, as seen in Fig. 4e (see also Fig. 5), the second internal solitary wave accumulates about 5% of the total initial wave energy, a figure comparable to the energy of the leading wave at its final stage, and this value hardly changes during 5 hours of evolution. In terms of wave amplitude, the two waves reveal more similar characteristics: at the final stage, their amplitudes are 17.5 and 16 m, respectively (see Fig. 6). So, this result illustrates the importance of

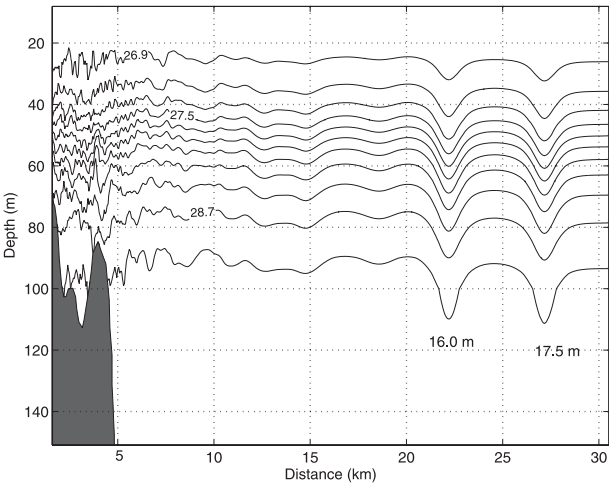

FIG. 6. Zonal cross section of density along 36°1.5′N (dashed line in Fig. 4e), showing the vertical structure of LAIWs entering the Alboran Sea. The time corresponds to that in Fig. 4e.

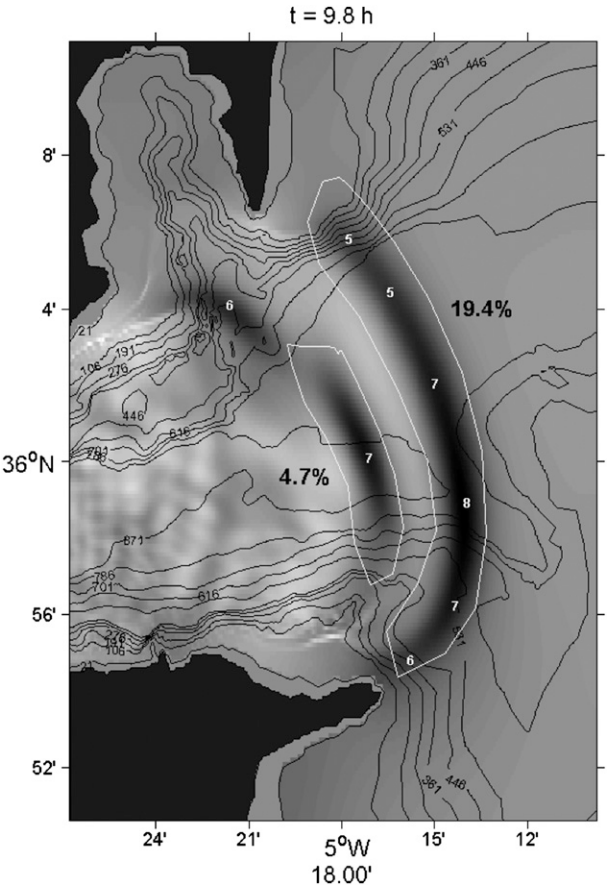

FIG. 7. As in Fig. 4, but for an initial solitary wave with 33-m amplitude.

the described mechanism of energy accumulation by the scattered waves.

The energy accumulation by secondary waves takes place in a wide range of initial wave amplitudes. As an example, Fig. 7 shows the resulting surface elevation produced by the internal solitary wave with initial amplitude of 33 m. During its propagation, this wave reveals a pattern of behavior very similar to the 3 times larger LAIW discussed above. The second newly generated solitary internal wave has an amplitude comparable with that of the leading LAIW, although it contains four times less energy due to a more compact spatial structure.

One last remark about the one-wave experiment concerns the generation of a system of relatively large internal waves that propagate across the strait. The energy flux in the incident wave directed initially from west to east (Fig. 4e) is, however, scattered by the strait in all other directions, producing cross-strait propagating internal waves. This system of randomly arranged waves is clearly seen in the far field of the wave pattern presented in Fig. 4e. They can also be identified in Figs. 6 and 7. The observational evidence of waves propagating northward was reported by Watson and Robinson (1991). The generation of cross-strait propagating waves is much stronger in the case of wave trains and is discussed in sections 3c and 3d in greater detail.

b. Influence of rotation

The internal Rossby radius of deformation in the Strait of Gibraltar is about 13.4 km, a value comparable to its width. Therefore, the contribution of the Coriolis force to the wave dynamics can be notable. An asymptotic analysis of the Ostrovsky equation (Ostrovsky 1978), which incorporates weak nonlinearity and rotational dispersion, shows that internal waves of permanent form cannot exist in rotating media (Leonov 1981). Being inserted into the model with rotation as an initial condition, a KdV solitary wave starts to radiate secondary waves (Gilman et al. 1996) and ultimately decays completely due to the permanent energy leakage (Grimshaw et al. 1998). There is however a strongly nonlinear limit of this theory that has been found recently by Helfrich (2007) and Grimshaw and Helfrich (2008). The fully nonlinear weakly nonhydrostatic equations from Choi and Camassa (1999) were generalized here to include weak rotation. It was found that in the case of strong waves not all of the energy of a LAIW is scattered to infinity due to the rotation dispersion. Part of it (up to 50%) can be accumulated in secondary waves generated from the evolution of the initial quasi-stationary LAIW. This process of generation of a compact packet of solitary-like waves from a single wave occurs as follows. At the first stage of evolution the

LAIW (which is the exact solution of the nonrotating Choi–Camassa equations) starts to decay, radiating inertia–gravity waves. These waves are eventually transformed into a packet of amplitude-modulated solitary waves that propagate through a long wave envelope. The group velocity of the envelope is less than the phase speed of every individual solitary wave. As a result, solitary waves emerge in the tail, propagate forward through the envelope, grow in amplitude to the middle of the packet, and then finally attenuate and decay at the leading edge. The instantaneous cross section of such a packet is non-rank-ordered but the LAIW has maximum amplitude in the middle of the packet. Such a wave train can be seen as modulated periodic waves (Helfrich 2007; Grimshaw and Helfrich 2008), or in the light of the present results, as a non-rank-ordered packet of solitary internal waves similar to that shown in Fig. 2d.

Another important factor in the evolution of LAIWs in the Strait of Gibraltar is the influence of lateral boundaries. Maxworthy (1983) first observed in the laboratory the transformation of an internal solitary wave due to rotation. Similar experiments were performed by Renouard et al. (1987), who reported the formation of a secondary wave train trailing the main wave. As a result of the energy transfer to the radiated waves, the internal solitary wave attenuates over the course of its propagation along the channel. A first theoretical explanation of this effect was given by Grimshaw (1985), who derived the rotation-modified Kadomtsev–Petviashvili equation assuming that the rotation effect is of the same order as nonlinearity and nonhydrostatic dispersion. Further theoretical and numerical analysis of this problem performed by Grimshaw and Tang (1990), and by Katsis and Akylas (1987), has shown that the Coriolis force gives rise to wave-front curvature and permanent radiation of secondary waves that leads to the decay of the initial wave due to radiation damping.

Within the context of the present paper the important outcome from all of the reported studies is that every internal solitary wave (propagating either along a channel or in the open sea) generates secondary waves due to rotation. In the case of several incoming waves the superposition of the many secondary wave systems can produce an irregular pattern with random distribution of wave amplitudes. Thus, the non-rank-ordered structure of the wave packets in the Strait of Gibraltar can be presumably explained (at least partly) by the action of the Coriolis force on a system of initially rank-ordered packets of LAIWs. The examination of this problem is the topic of the present section.

We start our analysis considering an idealized situation for a long straight channel of constant depth to exclude any influence of variable bottom topography. The input parameters for the MITgcm were close to the averaged values that occurred in the Strait of Gibraltar: the depth was equal to 600 m, the width 17 km, and the latitude 36°. The vertical fluid stratification and initial amplitude of the LAIW were the same as in the one-wave experiment in section 3a. Figure 8 represents the spatial distribution of amplitudes of the propagating LAIW and generated secondary wave tail after 10 hours of wave evolution (the typical time of wave propagation in the Strait of Gibraltar).

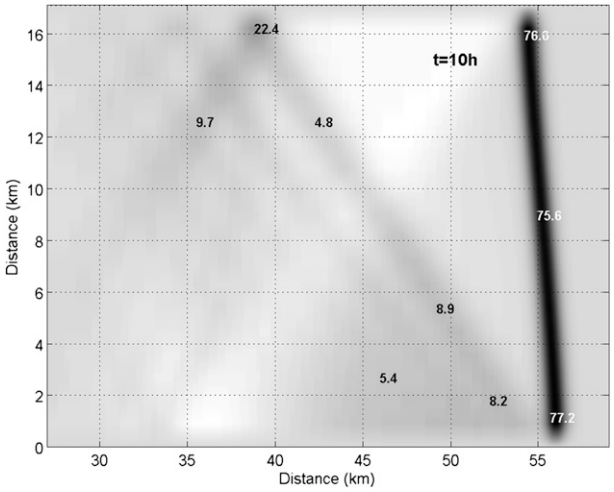

FIG. 8. Plan view of the wave field after 10-h evolution for the initial 83-m amplitude LAIW of depression in a rotating channel (36°N) of constant width (17 km) and depth (600 m). Small numbers indicate wave amplitudes (m).

The most obvious effects of rotation (Fig. 8) are the tilting of the wave front and the radiation of secondary waves, as predicted theoretically (Grimshaw 1985; Grimshaw and Tang 1990; Katsis and Akylas 1987). The effects are relatively weak and account for only 10% of the wave amplitude: after 10-h evolution the leading wave still predominates, its amplitude decreased by 6–8 m (from 83 to 77–75 m), and the amplitude of the radiated waves has this same order. The only area where secondary waves have noticeable amplitude (22.4 m) is located near the northern boundary due to wave reflection, but this local maximum (Mach stem) does not characterize the whole picture.

Other evidence of the weak response to the Coriolis force in Fig. 8 is the relatively slow decrease of the wave amplitude across the channel. The weakly nonlinear theory predicts an exponential decay of wave amplitude along its front (Grimshaw and Tang 1990; Katsis and Akylas 1987), which does occur for the set of input parameters considered here. This decay can be seen in Fig. 9, where the wave amplitude of the leading wave at three

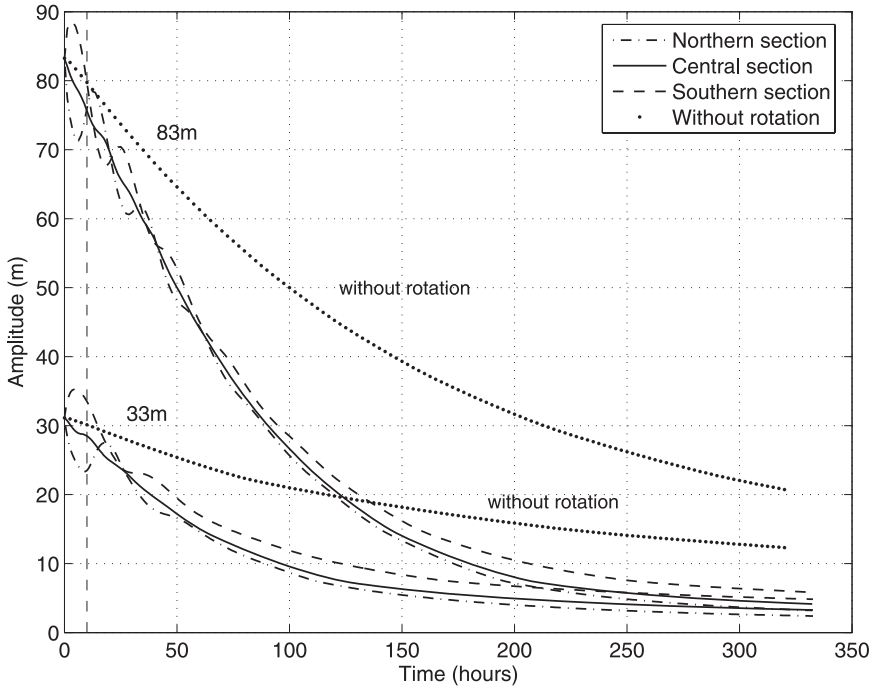

FIG. 9. Time evolution of the amplitude of the leading solitary wave calculated for two numerical runs (initial LAIW of depression of 83 and 33 m) in different zonal sections. The northern (southern) periphery of the wave is represented by the dashed–dotted (dashed) lines; the central section is shown by solid lines. The dotted lines correspond to the no-rotation experiment.

positions across the channel is presented. The wave amplitude decreases relatively quickly during the first 100–150 h, after which the leading LAIW tends to some kind of quasi-stationary state with the theoretically predicted exponential decay of amplitude across the channel (see Fig. 9 for $t > 100$ h). To ensure that the wave attenuation is not the consequence of viscous dissipation, the results of a numerical experiment without rotation are also presented in Fig. 9. The difference between rotation and no-rotation experiments (dotted and solid lines in Fig. 9) is clear evidence of the radiation damping of the leading wave induced by the rotation.

The described wave evolution scenario is valid across a wide range of amplitudes of incoming LAIWs (only two extreme runs with 83- and 33-m amplitude for the initial LAIW are presented in Fig. 9). For the objectives of the present study, an important result of these experiments is that the wave field does not change much during the first 10 h of LAIW evolution. Within 10%–15% accuracy, we can conclude that the wave amplitude in the domain remains basically the same (see the portion of the plot to the left of the vertical dashed line in Fig. 9), and the radiated waves are substantially weaker than the leading LAIW (Fig. 8). The change of the wave field owing to the Coriolis force is fairly weak because the time span of wave propagation (10 h) is not long enough for the development of any substantial rotational effect in the relatively narrow strait (its width, 17 km, is comparable to the internal Rossby radius of deformation, 13.4 km). In summary, one should not expect dramatic changes in the wave structure due to the rotation alone during the propagation of LAIWs along the Strait of Gibraltar. Figure 9 shows that we can expect some oscillations of amplitude across the channel in the range of about 10%–15% and predict the generation of a weak wave tail. Hence, any substantial modification of the wave form should be attributed to variations of the bottom topography. To verify this hypothesis, one extra numerical experiment without rotation has been performed for a LAIW with initial amplitude of 83 m and all other input parameters similar to those described for the one-wave experiment. The spatial structure of the leading LAIW and scattered secondary wave at selected moments in both runs, with and without rotation, are presented in Fig. 10. The comparison of these two experiments clearly shows some difference in the spatial structure of the rotational and nonrotational systems, such as the evident shift of the maximum amplitude area to the southern border during the first stages of evolution ($t = 6$ h). However, as seen from the latest

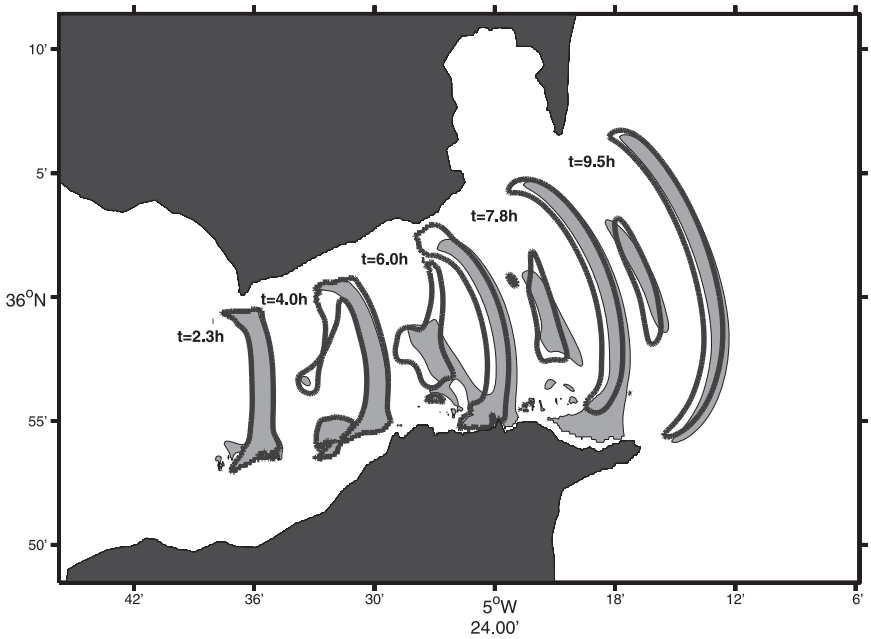

FIG. 10. Sea surface topography produced by 83-m amplitude LAIW of depression at different stages of evolution with and without rotation (shaded areas and thick contours, respectively). The contour of the 1.3-cm free-surface elevation was taken for both cases.

fragments ($t > 7.8$ h), the difference in the two wave patterns is not dramatic, suggesting that the formation of a scattered secondary wave tail in the Strait of Gibraltar is due to topographic effects, rather than to rotation.

c. *Evolution of wave trains: Two-wave experiment*

The results of the one-wave experiment give hints about the behavior of wave packets: the propagating LAIW radiates energy in the course of its evolution, and this process eventually leads to the formation of a second solitary wave with comparable amplitude. In the case of an initial wave train, the question then arises as whether the secondary waves radiated from the leading wave will propagate further independently (scenario 1) or if they will be absorbed by the subsequent incoming LAIWs (scenario 2). The answer can be found in Fig. 11 in which three stages of evolution of two initially isolated LAIWs are presented. The methodology of this experiment is the same as described in section 3a. The initial field in this experiment contains two LAIWs with amplitudes of 83 and 73 m for the leading and second waves, respectively, instead of a single wave. Two initial waves were separated by a distance of 3 km in order to be independent. Taking into account that the first, larger wave has the greater phase speed due to the nonlinear dispersion, there is no chance for their interaction in the course of propagation. However, the secondary waves produced by the first LAIW during the interaction with lateral boundaries can interfere with the second incoming wave. The implications of this interaction is the focus of the present section.

Wave patterns presented in Fig. 11 suggest that it is scenario 2 of the wave evolution that is realized. In other words, the waves radiated by the first LAIW near the strait boundaries are absorbed by the second LAIW. The energy absorption is so efficient that the second wave gets even larger than the first one, as shown in Figs. 11b and 11c. This scenario is also shown in Fig. 12 in which the evolution of the total energy of the two waves is presented. Of particular interest is the time span $t = 6$–7 h when the second wave contains two times more energy than the leading LAIW.

Notice that a third internal wave, which was expected to be generated in the course of superposition of secondary scattered waves, is not visible during most of the packet evolution. It is formed behind the first two waves only at the very end of the experiment when the packet leaves the strait (Fig. 11c). The energy of this third wave is remarkably less than the energy of the two leading waves and amounts to only 2.3% of the total initial energy. Obviously, the second LAIW also radiates part of its energy during propagation, but the energy supply from the first wave compensates this loss (the second wave attenuates more slowly than the first one at $t = 3$–6 h; see Fig. 12).

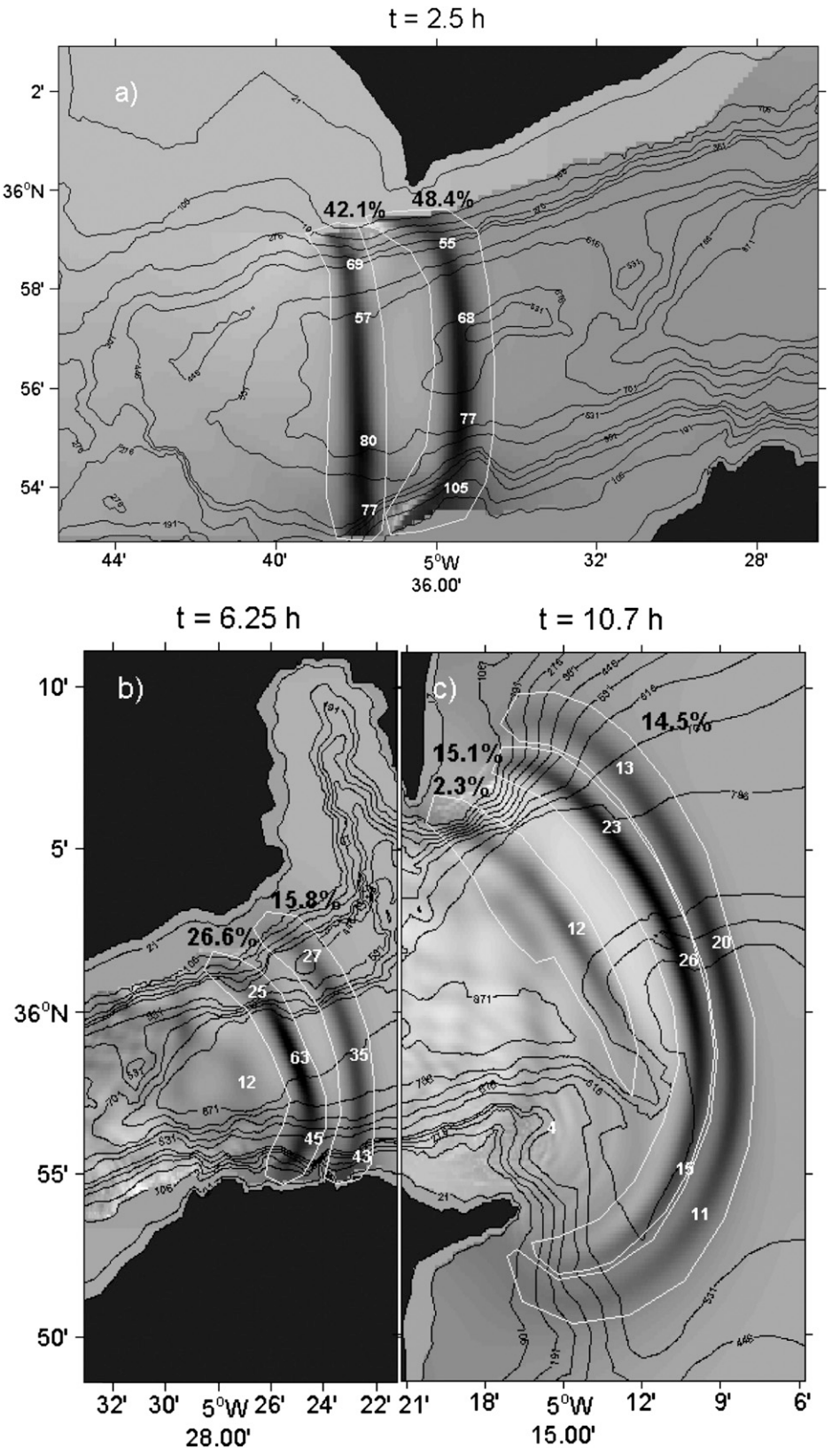

FIG. 11. As in Fig. 4, but for two propagating LAIWs with initial amplitudes of 83 and 73 m for the first and second waves, respectively.

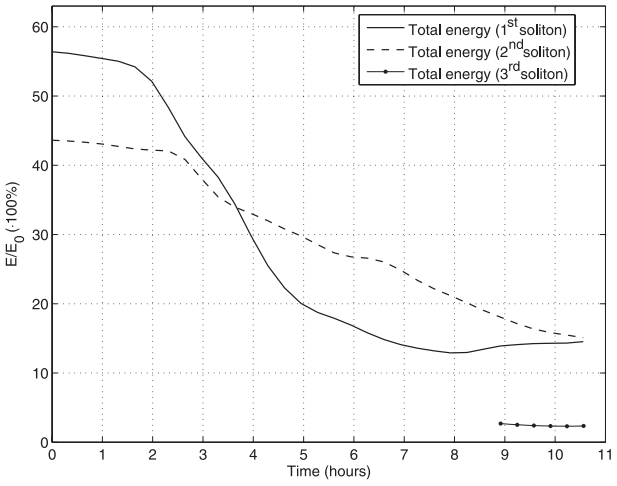

FIG. 12. Time evolution of the total energy of the leading and second LAIWs (solid and dashed lines, respectively) as well as the generated secondary internal solitary wave (dotted line), normalized by the energy of the two initial LAIWs.

Another effect, the wave–wave interaction, develops during the final stage of the packet evolution. The nonlinear collision of two internal solitary waves is possible when the leading wave is not the largest. In this case, the rear wave, with faster phase speed, starts to overtake the leading one. This overtaking eventually leads to the collision of the two internal solitary waves during which the rear wave transfers part of its energy to the leading wave. Figure 12 illustrates this process: after 8 h of evolution, the gradual attenuation of the leading LAIW is followed by a slow increase of its energy. This process was recently illustrated by Vlasenko and Stashchuk (2006, their Fig. 10).

d. Evolution of wave trains: Three-wave experiment

A new experiment with three initially rank-ordered LAIWs of amplitudes of 83, 73, and 63 m simulates the situation when three waves are generated over the CS. This run was organized in the same way as the two-wave experiment when LAIWs in the packet were well separated (3 km between waves), which excludes wave interaction at the initial stage.

Figures 13a and 13b show two intermediate stages of the packet evolution. Scrutiny of these two patterns, as well as their comparison with Figs. 4 and 11, allows one to conclude that the mechanism of energy transfer from the leading wave to the wave behind in the three-wave experiment works even more efficiently than that in the case of two waves. For instance, the total energy located in the first, second, and third waves, that is, 42.6%, 32.8%, and 24.6%, respectively, corresponding to the initial rank-ordered distribution of waves at $t = 0$, change dramatically. At $t = 7.7$ h (Fig. 13b), the energy remaining in the first, second, and third waves is 10.1%, 17.0%, and 13.9%, respectively. This fact clearly illustrates the inhomogeneity of energy dissipation along the train, from the leading LAIW to the wave tail. The second wave is the most energetic at $t = 7.7$ h, whereas the first one has lost most of its energy. At $t = 11.4$ h the second wave is no longer the strongest one. It contains 11.1% of the initial energy, whereas the first and third contain 11.1% and 6.7%, respectively. The first wave is now more energetic than 3.7 h before, a controversial result whose explanation has been mentioned above: the second LAIW has been accumulating most of the energy radiated by the leading wave and started to overtake it. Under such conditions the collision of two LAIWs becomes inevitable (this is especially clear in Figs. 13c and 14a), and, as a consequence of the wave–wave interaction, the second LAIW returns part of its energy back to the first one. The growth of the energy of the leading LAIW in Fig. 15 suggests that the collision of the two LAIWs starts about 8 h after the beginning of the experiment and that at $t = 11.4$ h, presented in Fig. 13c, the process is still in progress.

An interesting conclusion can be drawn from the analysis of the three-wave experiment: the third wave being less energetic in the global sense is, however, more compact in space and reveals the greatest local energy concentration. This fact is seen from comparison of the gray contrasts in Fig. 13c, as well as from Fig. 14a in which the zonal cross section of density along latitude 36°3.7′ is presented. The in situ measurements along this line would record a clear non-rank-ordered system of eastward-propagating progressive solitary waves in which the amplitude of the first wave is equal to 20 m, the second wave has amplitude 24 m, and the largest wave is the third one with amplitude ~30 m. This fact is in a good agreement with the observations of large internal waves registered at the AS mooring (see Fig. 2 and the appropriate discussion in the introduction).

4. Summary and conclusions

The results of the numerical simulations presented here illustrate a number of important aspects on the dynamics of tidally generated internal waves in the Strait of Gibraltar. In particular, it was found that initially plane LAIWs propagating along the strait reveal remarkable three-dimensional behavior. This effect is a direct consequence of many factors: one of which is the Coriolis force that initiates currents along wave fronts. Under the conditions of the constrained geometry these currents increase the wave amplitudes near the Moroccan coast, as seen in Figs. 4a–d and 11a,b. This is also confirmed by a comparison of the results obtained with

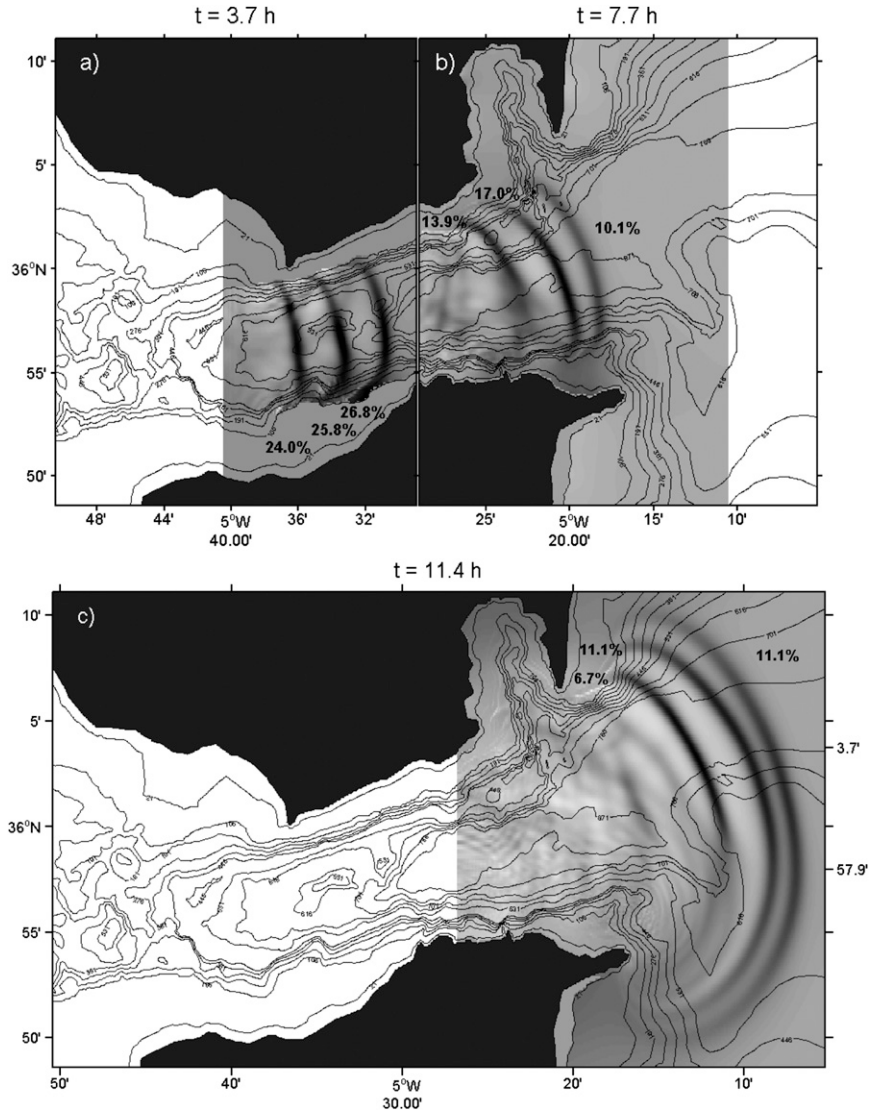

FIG. 13. Sea surface topography produced by a rank-ordered system of the LAIW of depression: initial amplitude of the propagating waves is 83, 73, and 63 m (from the right to the left), respectively. Percentages of energy are indicated.

and without rotation for the idealized rectangular channel presented in Fig. 9. The latter, in particular, illustrates that the initial tilting of the free surface produced by the Coriolis force across the channel is not stationary, but has an oscillatory character. The period of these cross-channel oscillations (following from Fig. 9) is about 22 h and the oscillations attenuate quickly (within two to three periods), being replaced by a stationary cross-channel sea surface tilting (Fig. 9 for $t > 50$ h). A similar effect of free-surface tilting was obtained analytically for the same idealized rectangle channel in the framework of a weakly nonlinear theory [Grimshaw (1985); Katsis and Akylas (1987); see also the review by Helfrich and Melville (2006) and references therein]. Our results expand this conclusion to the case of strongly nonlinear waves. Note also that the effect of rotation is fairly weak for the conditions in the Strait of Gibraltar and accounts for only 10% of the variability of wave amplitude across the strait (Fig. 9). Such a weak sensitivity to the Coriolis force is explained by the relatively short time of wave propagation: 10 hours of evolution is not long enough for the development of remarkable rotational effects (Fig. 10).

Another result found in the present study concerns the wave–wave energy transfer in internal wave packets propagating along the strait. Multiple reflections from lateral boundaries along with friction and wave breaking near the shoreline lead to attenuation of the propagating

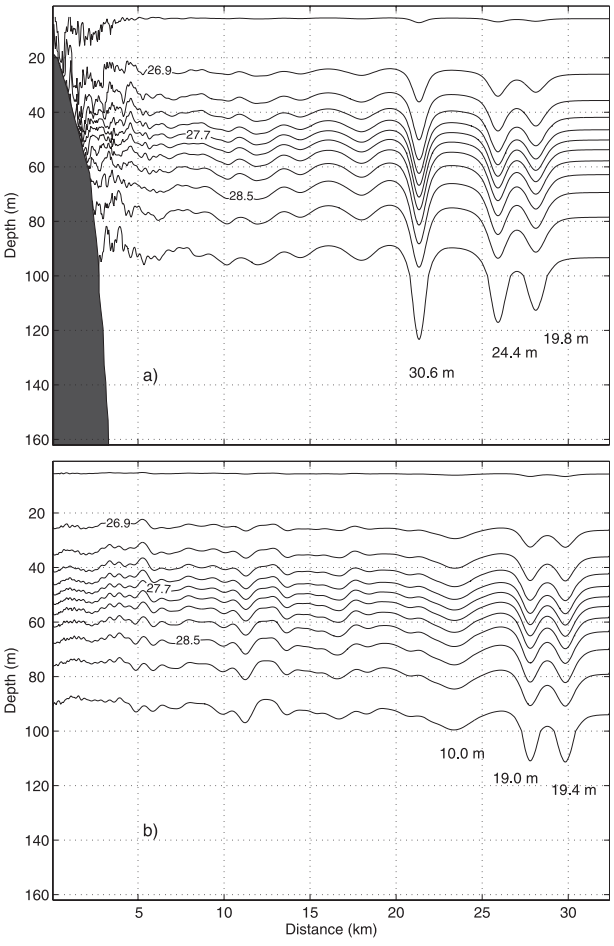

FIG. 14. (a) Zonal cross section of density along 36°3.7′N (see Fig. 13c) showing a non-rank-ordered system of LAIWs propagating eastward into the Alboran Sea. (b) A similar cross section along 35°57.9′N showing a well-rank-ordered system of LAIWs.

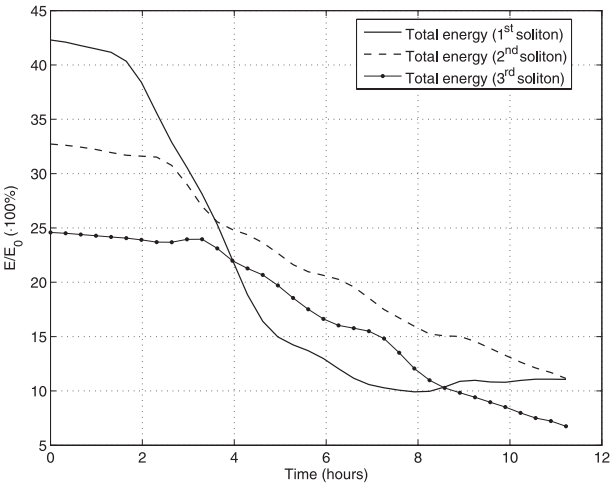

FIG. 15. Time evolution of the total wave energy of the three leading LAIWs.

waves. However, the leading LAIW loses its energy much faster than those in the wave tail (Fig. 15), as the latter absorb part of the energy scattered by the leading wave in the course of its evolution. As a result, the initially rank-ordered wave packet (the usual assumption for the generation mechanism) loses its regular structure and is transformed into a non-rank-ordered wave packet (Figs. 13 and 14a). This result is one of the major findings of the present study and deserves comment in greater detail.

The energy decay presented in Fig. 15 illustrates that at the first stage of evolution ($t < 3.5$ h) the wave packet maintains its initial rank-ordered structure even though the leading wave is losing energy at a very high rate. From 4 to 8.5 h the leading LAIW contains minimum energy in comparison with the other two, but after 8.5 h of evolution it starts to recover energy from the second wave. This is due to the energy transfer from the larger second wave that overtakes the first one, interacts with it, and transforms part of energy in the course of soliton–soliton interaction: a detailed description of this process for LAIWs can be seen in Vlasenko and Stashchuk (2006). At the end of the evolution, when the wave packet leaves the strait entering the Alboran Sea, its initial rank-ordered structure can be partly recovered due to wave–wave interaction but at a much lower energy level. Probably, this is the reason why almost half of all wave packets measured at the AS mooring (see Fig. 2) were well rank ordered or partly rank ordered. Generally speaking, the well-rank-ordered packets are expected to be the ultimate structure of all packets when they propagate long enough in a basin of constant depth.

The rank-ordered structure of wave packets arranged by energy does not necessarily mean a similar rank order in terms of wave amplitude. This effect takes place because of substantial three-dimensionality of the problem. In fact, the total energy accumulated by the leading LAIW in the whole domain does not guarantee that this wave contains the local energy maximum. In some cross sections, the amplitudes of successive waves can be larger so that the greatest amplitudes can be recorded in the less energetic (in a global sense) wave.

Such an example is illustrated in Fig. 14 in which two cross sections of the same wave packet are presented: the cross section in Fig. 14a is for $t = 11.4$ h (see Fig. 13c) along latitude 36°3.7′, whereas Fig. 14b is for latitude 35°57.9′. The third wave in Fig. 14a has the maximum amplitude despite the fact that it is the least energetic wave in the packet (Figs. 13c and 15). This contradictory result can be explained in terms of cross-strait variability of the wave (see Fig. 11b), which is a consequence of the Coriolis force and three-dimensional effects. These

results can be a matter for further scrutiny, which is necessary to reach the correct interpretation of in situ observations when the data collected at different sites in the packet can lead to opposing conclusions. It is also interesting to mention the sharp decrease in the wave amplitude at the southern periphery of the waves as they radiate out from the strait. This fact is obviously related to the sudden change in the shoreline orientation near 5°16′W.

The structure of wave packets in the strait is substantially dependent on the position of the observer. At two different fixed points the same wave train can reveal either well-rank-ordered or rather irregular structures. The local organization of amplitude ranking cannot be inferred directly from the energy content, as a more global variable. From the viewpoint of the observations, this randomness would explain the similar proportion of rank- and non-rank-ordered LAIWs packets found in the temperature records at the AS mooring (Figs. 1 and 2). It is expected that these results, obtained for the Strait of Gibraltar, will also be valid for other straits of the World Ocean.

Acknowledgments. The authors are grateful to three anonymous referees for useful comments and suggestions. This work was supported by U.K. NERC Grant NE/F010214/1 (Nontraditional baroclinic wave effects in the Strait of Gibraltar). JCSG acknowledges a postgraduate fellowship from Consejeria de Innovacion Ciencia y Empresa, Junta de Andalucia, Spain (Project RNM 968). Partial support from Spanish National Project CTM2006-02326/MAR is also acknowledged. We are thankful to Dr. Javier Delgado for providing the bathymetry map.

APPENDIX A

Calculation of Wave Energy

Let us define $\rho_B(z)$ as the background unperturbed density profile (see Fig. 3). The three-dimensional fields of density and velocity associated with the internal wave perturbations are defined as ρ and $\mathbf{u} \equiv (u, v, w)$, respectively. Defining $\xi(x_0, y_0, z_0)$ as the vertical excursion of the fluid particle from the equilibrium position (x_0, y_0, z_0), the work per unit volume W_p required to displace the particle from z_0 to $z_0 + \xi_0$ reads

$$W_p = -g \int_{z_0}^{z_0+\xi_0} [\rho_B(z_0) - \rho_B(z)]\, dz, \qquad \text{(A1)}$$

where g is the acceleration due to gravity. For infinitesimal waves, the above expression can be computed by taking a Taylor expansion of $\rho_B(z)$ centered at $z = z_0$. With first-order accuracy, it can be found that

$$W_p = \rho_B(z_0) \frac{N^2(z_0)}{2} \xi_0^2.$$

However, for the large-amplitude internal waves analyzed here, this approximation is not valid, and (A1) has been computed using the standard trapezoidal integration technique.

The total energy E_T of the internal wave is obtained by integrating the energy within the fluid volume V that includes the wave. Thus, the total energy is $E_T = E_{AP} + E_K$, where E_{AP} and E_K are the available potential and kinetic energies, respectively (Vlasenko and Stashchuk 2007). They are calculated separately according to the formulas $E_{AP} = \int_V W_p\, dV$ and $E_K = \frac{1}{2} \int_V \rho(u^2 + v^2 + w^2)\, dV$.

APPENDIX B

Influence of the Mean Current

The results presented here were obtained in the absence of a mean flow—the key feature of the Strait of Gibraltar. Note, however, that we are focusing on the internal wave evolution along the strait, which is not always sensitive to weak along-strait variations of the current. In many cases the weak horizontal gradients normally lead to the adiabatic adjustment of the waves. Such a conclusion was formulated by Vlasenko et al. (2005a) for an internal wave propagating over weakly varying bottom topography. To ensure that this is the case in the present study, that is, the steady-state current in not a major issue in the discussed problem, an extra numerical experiment was performed. Figure B1 shows the wave propagating along a rectangular channel without rotation with a background baroclinic, two-way current typical for the Strait of Gibraltar. The fluid stratification was similar to that used in the basic series of runs (the top panel in Fig. B1 represents only one isopycnal for the sake of clarity). The along-strait gradient of density was produced by the mean current–countercurrent shear flow initiated in the model. It is clear from Fig. B1 that the propagation in the background of the mean current LAIW simply adjusts to the ambient conditions without disintegration. The background current does affect the wave characteristics, but in the context of the present paper it is important to note that the propagating wave does not radiate any secondary wave (see Fig. B1) and cannot affect the major conclusions of the paper.

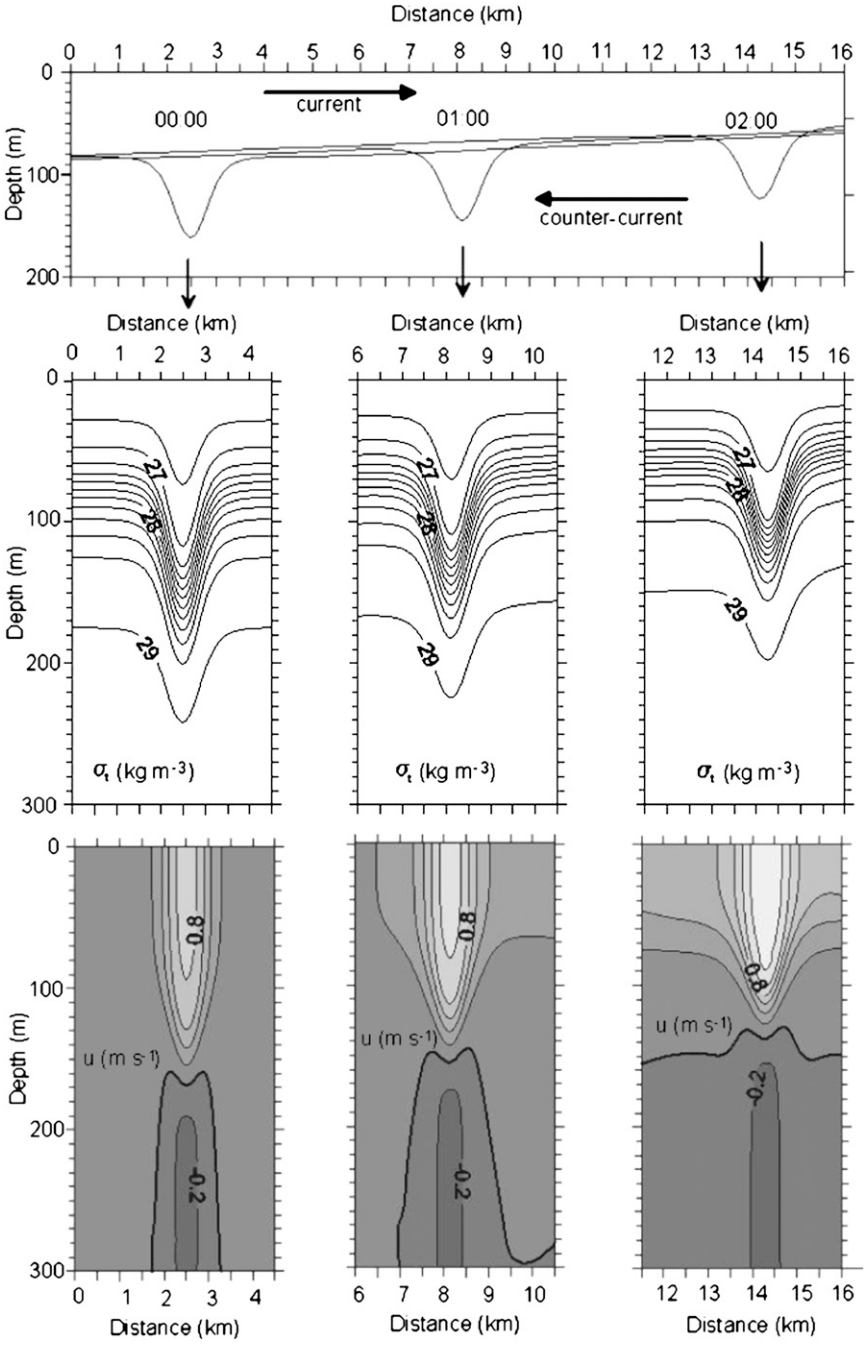

FIG. B1. (top) Three stages of evolution of an LAIW with amplitude 83 m along a rectangular channel 600 m deep (only $\sigma_t = 28$ kg m^{-3} is plotted). The water stratification and the current–countercurrent flow were taken close to those observed in the Strait of Gibraltar. Detailed structures of the (middle) density and (bottom) horizontal velocity fields for every time span.

REFERENCES

Apel, J., 2003: A new analytical model for internal solitons in the ocean. *J. Phys. Oceanogr.,* **33,** 2247–2269.

Armi, L., and D. Farmer, 1988: The flow of the Mediterranean water through the Strait of Gibraltar. *Prog. Oceanogr.,* **21,** 1–105.

Brandt, P., W. Alpers, and J. O. Backhaus, 1996: Study of the generation and propagation of internal waves in the Strait of Gibraltar using numerical model and synthetic aperture radar images of the European ERS-1 satellite. *J. Geophys. Res.,* **101,** 14 237–14 252.

Bruno, M., J. Alonso, A. Cozar, J. Vidal, F. Echevarria, J. Ruiz, A. Ruiz-Canavate, and A. Gomez, 2002: The boiling water

phenomena at Camarinal Sill, the Strait of Gibraltar. *Deep-Sea Res. II,* **49,** 4097–4113.

Choi, W., and R. Camassa, 1999: Fully nonlinear internal waves in a two-fluid system. *J. Fluid Mech.,* **396,** 1–36.

Gilman, O. A., R. Grimshaw, and Yu. A. Stepanyants, 1996: Dynamics of internal solitary waves in a rotating fluid. *Dyn. Atmos. Oceans,* **23,** 403–411.

Grimshaw, R., 1985: Evolution equation for weakly nonlinear, long internal waves in a rotating fluid. *Stud. Appl. Math.,* **73,** 1–33.

——, and W. Melville, 1989: On the derivation of the rotation-modified Kadomtsev–Petviashvili equation. *Stud. Appl. Math.,* **80,** 183–202.

——, and S. Tang, 1990: The rotation-modified Kadomtsev–Petviashvili equation: An analytical and numerical study. *Stud. Appl. Math.,* **83,** 223–248.

——, and K. R. Helfrich, 2008: Long-time solutions of the Ostrovsky equation. *Stud. Appl. Math.,* **121,** 71–78.

——, J.-M. He, and L. Ostrovsky, 1998: Terminal damping of a solitary wave due to radiation in rotational systems. *Stud. Appl. Math.,* **101,** 197–210.

——, E. Pelinovsky, and A. Polukhina, 2002: Higher-order Korteweg–de Vries models for internal solitary waves in stratified shear flow with a free surface. *Nonlin. Processes Geophys.,* **9,** 221–235.

——, ——, T. Talipova, and A. Kurkin, 2004: Simulation of the transformation of internal solitary waves due on oceanic shelves. *J. Phys. Oceanogr.,* **34,** 2774–2791.

Helfrich, K. R., 2007: Decay and return of internal solitary waves with rotation. *Phys. Fluids,* **19,** 026601, doi:10.1063/1.2472509.

——, and W. K. Melville, 2006: Long nonlinear internal waves. *Annu. Rev. Fluid Mech.,* **38,** 395–425.

Izquierdo, A., L. Tejedor, D. Sein, J. Backhaus, P. Brandt, A. Rubino, and B. Kagan, 2001: Control variability and internal bore evolution in the Strait of Gibraltar: A 2-D two-layer model study. *Estuarine Coastal Shelf Sci.,* **53,** 637–651.

Katsis, C., and T. R. Akylas, 1987: Solitary internal waves in a rotating channel: A numerical study. *Phys. Fluids,* **30,** 297–301.

La Violette, P., T. Kinder, and D. Green III, 1986: Measurement of internal waves in the Strait of Gibraltar using a shore-based radar. Naval Ocean Research and Development Activity Rep. 118, 13 pp.

Leonov, A. I., 1981: The effect of the earth's rotation on the propagation of weakly nonlinear surface and internal long waves. *Ann. N.Y. Acad. Sci.,* **373,** 150–159.

Marshall, J., A. Adcroft, C. Hill, L. Perelman, and C. Heisey, 1997: A finite-volume, incompressible Navier–Stokes model for studies of the ocean on parallel computers. *J. Geophys. Res.,* **102,** 5733–5752.

Maxworthy, T., 1983: Experiments on solitary internal Kelvin waves. *J. Fluid Mech.,* **129,** 365–383.

Ostrovsky, L. A., 1978: Nonlinear internal waves in a radiating ocean. *Oceanology (Moscow),* **18,** 119–125.

Pacanowski, R. C., and S. G. H. Philander, 1981: Parameterization of vertical mixing in numerical models of tropical oceans. *J. Phys. Oceanogr.,* **11,** 1443–1451.

Renouard, D. P., G. Chabert d'Hieres, and X. Zhang, 1987: An experimental study of strongly nonlinear waves in a rotating system. *J. Fluid Mech.,* **177,** 381–394.

Sanchez Garrido, J. C., J. Garcia Lafuente, F. Criado Aldeanueva, A. Baquerizo, and G. Sanino, 2008: Time-spatial variability observed in velocity of propagation of the internal bore in the Strait of Gibraltar. *J. Geophys. Res.,* **113,** C07034, doi:10.1029/2007JC004624.

Sanz, J. L., J. Acosta, M. Esteras, P. Herranz, C. Palomo, and N. Sandoval, 1991: Geophysical survey of the Strait of Gibraltar (results of the Hercules program 1980–1983). Special Publications of the Spanish Institute of Oceanography, Vol. 7, 48 pp.

Vazquez, A., N. Stashchuk, V. Vlasenko, M. Bruno, A. Izquierdo, and P. Gallacher, 2005: Evidence of multimodal structure of baroclinic tide in the Strait of Gibraltar. *Geophys. Res. Lett.,* **33,** L17605, doi:10.1029/2006GL026806.

Vlasenko, V., and N. Stashchuk, 2006: Amplification and suppression of internal waves by tides over variable bottom topography. *J. Phys. Oceanogr.,* **36,** 1959–1973.

——, and ——, 2007: Three-dimensional shoaling of large-amplitude internal waves. *J. Geophys. Res.,* **112,** C11018, doi:10.1029/2007JC004107.

——, L. Ostrovsky, and K. Hutter, 2005a: Adiabatic behavior of strongly nonlinear internal solitary waves in slope-shelf areas. *J. Geophys. Res.,* **110,** C04006, doi:10.1029/2004JC002705.

——, N. Stashchuk, and K. Hutter, 2005b: *Baroclinic Tides: Theoretical Modeling and Observational Evidence*. Cambridge University Press, 375 pp.

Watson, G., and I. Robinson, 1990: A study of internal wave propagation in the Strait of Gibraltar using shore-based marine radar images. *J. Phys. Oceanogr.,* **20,** 374–395.

Wesson, J., and M. Gregg, 1988: Turbulent dissipation in the Strait of Gibraltar and associated mixing. *Small-Scale Turbulence and Mixing in the Ocean,* J. Nihoul and B. Jamart, Eds., Elsevier Oceanography Series, Vol. 46, Elsevier, 201–212.

Whitham, G., 1974: *Linear and Nonlinear Waves*. Wiley and Sons, 636 pp.